ORIGINAL PAPER

Corrosion protection of AA6061-T4 alloy by sol–gel derived micro and nano-scale hydroxyapatite (HA) coating

S. Sonmez · B. Aksakal · B. Dikici

Abstract Micron and nano-scale hydroxyapatite (HA) were coated successfully on AA6061-T4 substrates by sol–gel method. Besides, the effects of coating thickness on adhesion strength and corrosion behaviour of the coatings were studied. Corrosion resistance was measured by potentiodynamic polarization test using a potentiostat under in vitro conditions. The coatings before and after corrosion tests were characterized by adhesion tests, a scanning electron microscopy attached with EDS and X-ray diffraction analysis. The results revealed that all the coatings exhibit a passive behaviour in Ringer's solution. Specimens coated with nano-scale HA had the higher corrosion resistance than micro-scale coatings. The highest corrosion resistance appeared to be for the ∼ 30 μm nano-scale HA coated substrates. However, for micro-scale HA coatings, the highest adhesion resistance was obtained at ∼ 30 μm film thickness.

Keywords Hydroxyapatite · A6061-T4 · Sol–gel · Corrosion

S. Sonmez
Department of Biomedical Engineering, Hakkari University, 30000 Hakkari, Turkey

B. Aksakal (✉)
Department of Metallurgy and Material Engineering, Yildiz Technical University, 34349 Beşiktaş, Istanbul, Turkey
e-mail: baksakal2@gmail.com

B. Dikici
Department of Mechanical Engineering, Yuzuncu Yil University, 65080 Van, Turkey

1 Introduction

Metallic materials are increasingly used in medical applications as implants to restore some damaged and lost functions of body parts and joints or to replace organs functioning at acceptable levels. Recently, Ti alloys, 316L stainless steel and Co–Cr alloys have been the most attractive biomaterials due to their good corrosion resistance, biocompatibility, greater specific strength and much lower elastic modulus than the other metallic biomaterials [1–5]. However, Ti alloy implants may lead to potentially serious health problem because some ions in the alloys have been found to cause cytotoxic effects and adverse tissue reactions [6, 7]. Most researches focused on improving the adhesion strength of the implant-tissue interface. Thus, calcium phosphate (CaP) based coatings was performed to improve bone ingrowths when implanted in body. It has been well known that hydroxyapatite (HA) $[Ca_{10}(PO_4)_6(OH)_2]$ is bioactive and biocompatible with human hard tissues. Unfortunately, the mechanical properties of hydroxyapatite are fairly poor and cannot be used directly as implants in load bearing applications [8–12].

The physiological environment (body fluid) is considered extremely corrosive to metallic surfaces and corrosion is one of the major problems to the widespread use of the metals in the human body [13]. Metallic biomaterials corrode in variety of ways including general and localized corrosion types in which pertinent to the currently used alloys such as galvanic, pitting, crevice, intergranular, stress-corrosion cracking, corrosion fatigue and fretting corrosion. The biocompatibility of the metallic implant is one of considerable concern because these implants are exposed to corrosion during in vivo environment [14]. Mechanical properties such as tensile strength, fracture toughness and especially elastic modulus of the implant, must be considered [15]. On top of

this, aluminium is an extremely light material having low density, high specific strength, stiffness, good castability and machinability and high damping capacity [16]. In addition, it has good corrosion resistance due to formation of an inert oxide layer on its surface. 99.5 % pure alumina (aluminium oxide) according to the ASTM specifies, the Al_2O_3 substances can be used for implant applications [17]. Its high hardness is accompanied by low friction and wear and inertness to the in vivo environments could be attractive for biomedical applications. The elasticity modulus of cortical bone is 10–50 times less than that of Al_2O_3 [12], but closer than those Ti and stainless steel materials. However, due to its brittleness, direct use of Al_2O_3 as implant material is not possible, nevertheless the need to reduce costs in public health services may compel the use of specially treated other aluminium alloys e.g. coated by HA as the most economical alternatives for implants. However, the knowledge about the Al substrate as implant, including HA particle size and coating thickness on the corrosion resistance of Al substrates is very limited.

Recently, many methods have been used to produce HA coating on implant surfaces. The sol–gel derived dip coating process provides attractive alternative coatings because of the homogeneity due to atomic level mixing, easy formation of crystalline films at relatively low temperature, offering the possibility to tailor microstructures [9–11, 18–23]. In addition, its convenience for complex shape coatings and technical simplicity at lower production costs, compared to the other processes such as plasma spray [24], dip coating [25], electrophoretic deposition (EPD) [26, 27], plasma immersion ion implantation and deposition [28], and magnetron sputtering [29].

In order to demonstrate a possible alternative usage of Al alloys in low load bearing biomedical applications, the adhesion strength and corrosion resistance of sol–gel derived Hydroxyapatite Based Bioceramic (HABC) dipcoating on A6061-T4 alloy is presented in this work. Besides the adhesion, the effects of hydroxyapatite particle size and coating thickness on corrosion behaviour of the coatings were studied.

2 Experimental procedure

2.1 Material

The chemical composition of the A6061-T4 substrate used in this study is shown in Table 1. The specimens were cut off from Al alloy sheets having the dimensions of $10 \times 10 \times 2.3$ mm. HABC coatings of Al substrates were prepared by means of sol–gel technique. Before the coating process, the substrates were sand blasted by silica beads with particle size of approximately 100 μm. The substrates were thoroughly washed with a detergent, then ultrasonically cleaned twice with acetone for 10 min, and passivated in nitric acid for 3 h. Then, the substrates were again cleaned ultrasonically with ethanol for 10 min and dried in air. The specimens were divided into two groups. The adhesion tests were applied to the first group and corrosion tests to the second group. All substrates in both groups have been HABC coated in three different coating thicknesses by micron (35 μm, Merck) and nano (20 nm) scale-HA powders (Sigma–Aldrich).

2.2 HABC coatings

In order to determine the effect of HABC coatings on corrosion behaviour of the substrates, coating thickness and HA particle sizes were selected as variables. For the coating, $10 \times 10 \times 2.3$ mm specimens were cleaned in detergent, 25 % nitric acid and acetone then ultrasonically cleaned and dried in air, respectively. Before dip coating, the suspension was prepared in a 125 ml beaker by using inorganic chemicals (Sigma-Aldrich) such as HA (35wt.%), P_4O_{10} (30wt.%), $CaCO_3$ (20wt.%), CaO (10wt.%) and 5wt.% $KH_2(PO_4)$. They were mixed in ethanol (99.8 %) and distilled water at given concentrations and the obtained suspension was stirred on a hot plate for 20 min. Then, the prepared suspension was ultrasonically homogenized (Cole-Parmer-750Watt) for 15 min at room temperature. The sand blasted and cleaned Al substrates were then dip coated. Three ascending and immersion times (2.5, 5 and 10 mm/s) and two different HA powder sizes (35 μm and 20 nm) were used during dipping process. The coating took place by using nano and micro scale-HA at different dipping times of 1, 2 and 4 s. The coating thicknesses were determined directly from the observed cross-section of the coatings via SEM. They were finally sintered at 520 °C for 30 min. in a horizontal sintering furnace under a vacuum. To determine the adhesion strength between coat and substrate and also to show the corrosion resistance, the coated specimens were subjected to adhesion and corrosion tests.

2.3 Adhesion tests

Adhesion strength of the HABC coated Al strip substrates having the dimensions of $32 \times 18 \times 2.3$ mm in

Table 1 Chemical composition of the AA6061-T4 substrate

Substrate	Fe	Si	Mn	Cr	Cu	Zn	Al	Mg
wt.%	0.436	0.572	0.047	0.113	0.282	0.021	97.17	1.356

which coated at the same conditions and for three different coating thicknesses (~ 30, ~ 60, ~ 85 μm). The tests were executed by a tensile test machine (50 kN, Shimadzu, Japan) according to ASTM 370. Thirty-six strip specimens and three specimens for each tests were used in total. FM 73 toughened epoxy (47 MPa) was applied on one side of the coated surfaces of the coated strips.

2.4 Corrosion tests

Corrosion resistance of the HABC coatings has improved by the formation of thin and dense oxide films (passive films) over the surfaces of the implants. The passive film formation and stability are usually evaluated by anodic polarization tests [7]. Therefore, electrochemical investigations of the coatings were performed with potentiodynamic scanning (PDS) technique. All experiments were carried out with a computer-controlled potentiostat (PCI4/750, GAMRY Instruments, Inc., Warminster, PA) in Ringer's solution at body temperature (37 °C $\pm$ 0.1). Ringer's solution is commonly used for in vitro corrosion studies in biomaterials because it simulates physiological media of human body fluid. Ag/AgCl and platinum (Pt) wire electrodes were used as a reference and auxiliary electrode, respectively. The specimens with a square surface area of 1 cm^2 were used and the working electrode were embedded with cold resin and ultrasonically cleaned in distilled water. During the corrosion tests, firstly, the specimens were immersed into the solution until reaching a steady open circuit potential (OCP) to obtaining PDS curves. After equilibration, the PDS began at the cathodic overpotential of -250 mV versus E_{ocp} at a rate of 1 mV/s until the pitting potential (E_{pit}) was observed. The scan was stopped when the specimens reached to an anodic current density of 10 mA/cm^2. All electrochemical tests were repeated three times and the reproducibility of the polarization curves was determined in the variation of ± 5 mV. However, the reproducibility of the nano scale HA coatings was better than micro scale-HA coatings.

2.5 Surface analysis

Before and after corrosion tests, the specimens were cleaned ultrasonically in distilled water and dried in cold air for microstructural observations. Microstructural characterization studies were carried out by using a scanning electron microscope (SEM) (Jeol JSM–7001F) and electron dispersive spectroscopy (EDS). Also, the coatings were characterized by X-ray diffraction technique (XRD, Rigaku RadB-DMAX II).

3 Results and discussion

In this section, the coated samples are denoted with an identifiable code for easy expression, e.g. two different HA powder sizes (35 μm and 20 nm) were used for production of coatings. The coated samples were named and derived from the powder particle sizes given as M (micro, 35 μm) and N (nano, 20 nm), respectively. The coating took place by using different dipping times of 1, 2 and 4 s with obtained corresponding thicknesses of 30 ($\pm$2), 60 ($\pm$2) and 85 μm ($\pm$2), respectively. Therefore, coating thickness values were named as M30 which represents the coating thickness of 30 μm by using micro-scale (35 μm) HA powders, and N30 represents the coating thickness of nano-scale (20 nm) HA particles.

3.1 Surface

The XRD technique is more suitable for the chemical analysis of surface constituents whose depth is between 10 and 100 μm from the outermost surface of a specimen [30]. The XRD patterns of the M30 and N30 coatings are shown in Fig. 1. The XRD peaks reveal that two coatings (micro or nano) exhibit the same structure after the sol–gel coatings. The analysis confirmed HA formation on the surface of the coatings with crystallized hydroxyapatite crystal peaks and intermetallic compounds or other phases were not detected. Figure 2 shows the typical microstructure of M30 and N30 coatings. SEM observations revealed that the surface of the coatings was homogeneous and dense in appearance and that some cracks were observed as shown in Fig. 2a, c. Higher magnifications of HABC coatings are porous and they appear like cauliflowers (Fig. 2b, d).

SEM images at different magnifications and its EDS spectrum of the M85 and N85 specimens is illustrated in Fig. 3, where indicates the elemental composition of the coated substrate. Intense peaks for calcium and phosphorous were obtained as expected. The intense peaks for Ca, P and O suggest the presence of bioceramic coating
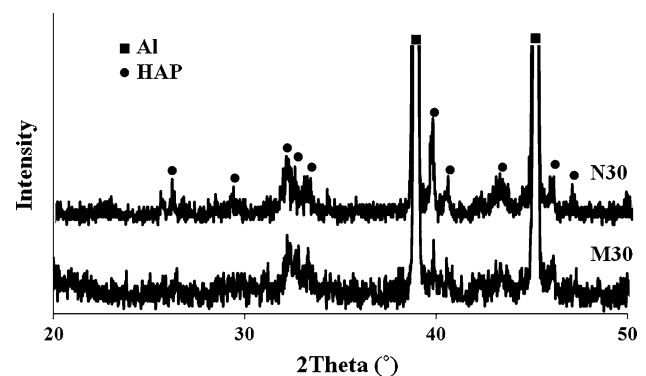

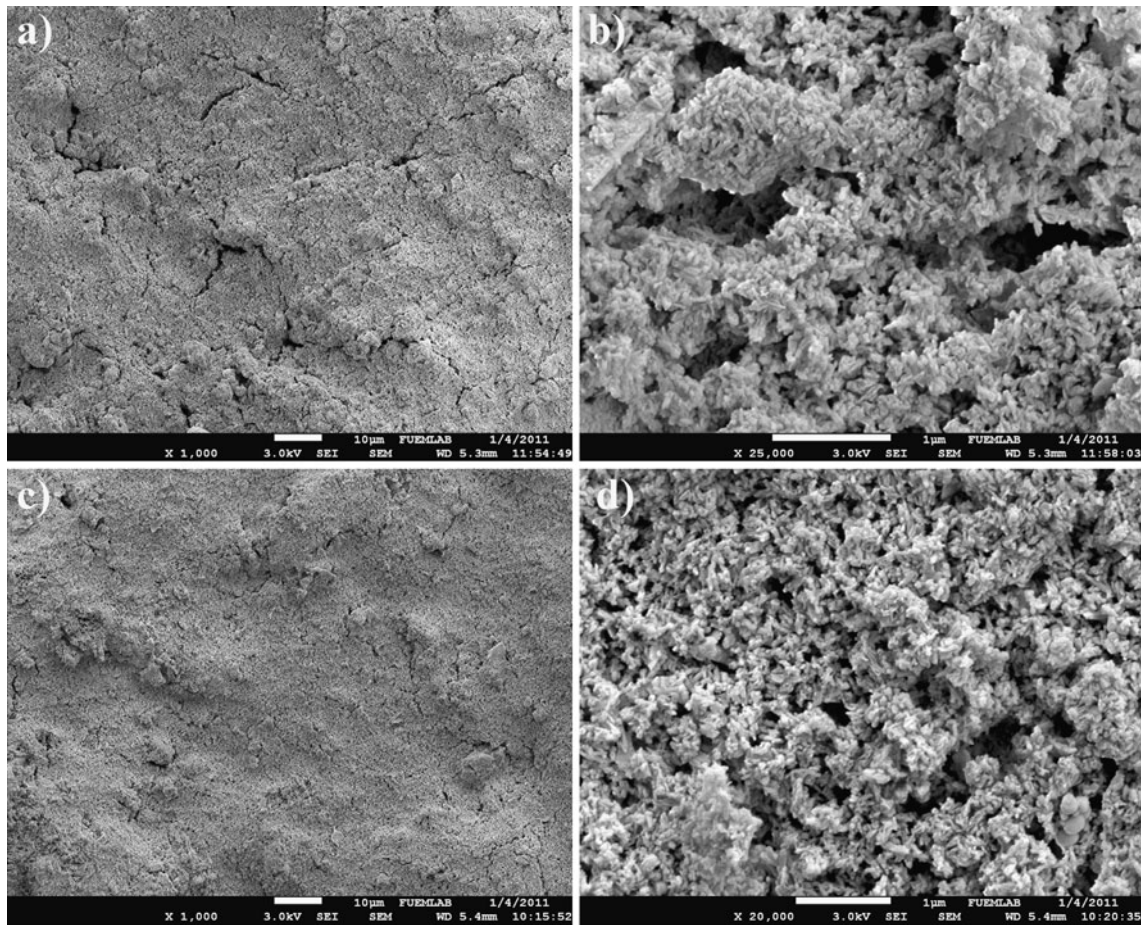Fig. 1 XRD patterns of the M30 and N30 coatings

Fig. 2 SEM micrographs of the M30 and N30 coatings using micro and nano HAP particles: **a** at low magnification (M30), **b** at high magnification (M30), **c** at low magnification (N30), and **d** at high magnification (N30)

[31–33]. Also, synthetic bioactive calcium phosphate compounds with various calcium and phosphate ratios were discussed comprehensively in many research papers. According to studies, calcium phosphate can be crystallized into different forms (such as mono-, di-, tri-, and tetra-calcium phosphates, hydroxyapatite, and β-whitlockite) depending on the Ca/P ratio, presence of water, impurities, and temperature. Besides, synthesis conditions influence very strongly crystal size of calcium phosphate based coatings. According to the EDS analysis of the coated substrates, Ca/P ratio values of the coatings of M85 and N85 were calculated to be 1.998 and 2.236 respectively. It is seen from the results that Ca/P ratios of the coatings were fairly deviated from the stoichiometric Ca/P (1.67) ratio of the HA, both of closely correspond to tetracalcium phosphate (TTCP). It is well known that the Ca/P ratio of the final HA depends on the ratio between the starting components. Probably, it can be thought that incorporation of some silicate ions into some phosphate ions give rise to increment of Ca/P ratio [17, 34–36].

SEM images and the EDS spectrum show that the increase in dipping time caused the morphology to form a denser and more porous structure. In addition, the coated samples with micro-scale HA particles present similar morphology with less porous structure for nano-scale HA particles. Porosity is always required for biocompatible implants because living cells need such scaffolds to proliferate and nutrition can be supplied as cells migrate into to the porous space. As indicated in Fig. 3b, e, the morphology of the coated specimens with nano-scale HA particles has a porous and less cracked structure than the coated specimens with micro HA particles which is essential for implant longevity. However, the existence of cracks causes a loss in structural integrity of the coating.

3.2 Adhesion

The variation of adhesion strengths of HABC coated Al substrates with respect to HA particle size and coating thickness are shown in Fig. 4. The coatings exhibit different adhesion values due to different volume fraction of
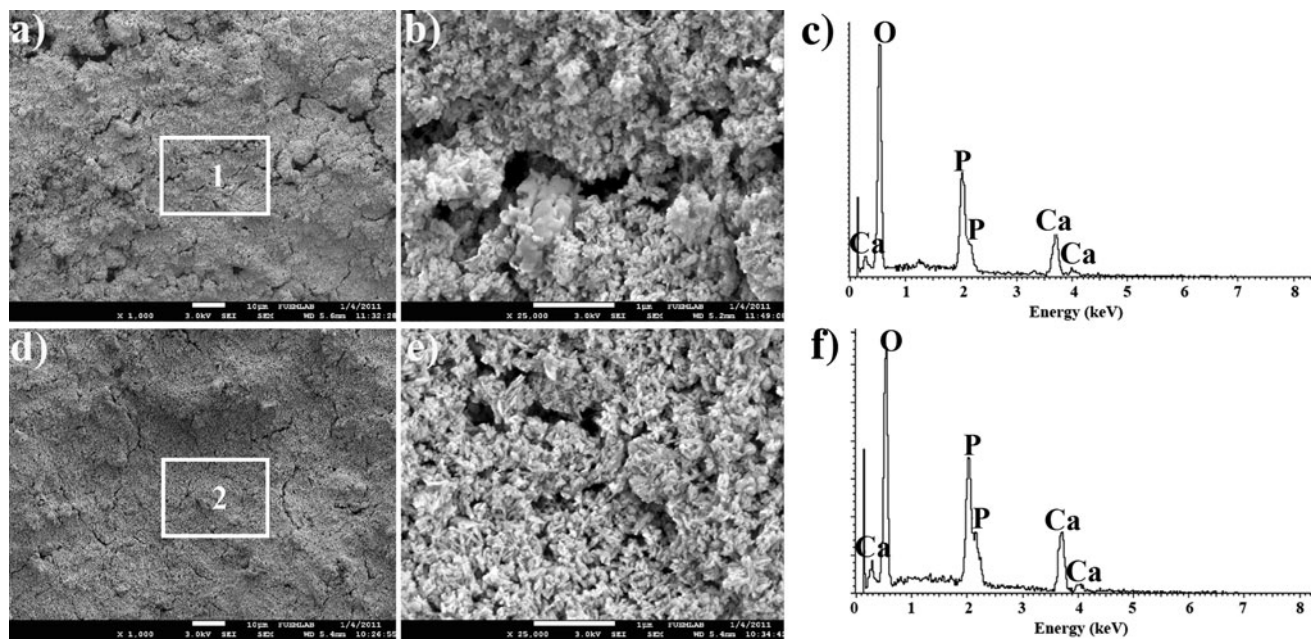
Fig. 3 SEM micrographs and EDS spectrum of M85 and N85 coatings: **a** at low magnification, **b** at high magnification, **c** EDS analysis of region 1, **d** N85, **e** at high magnification of N85 and **f** EDS analysis of region 2
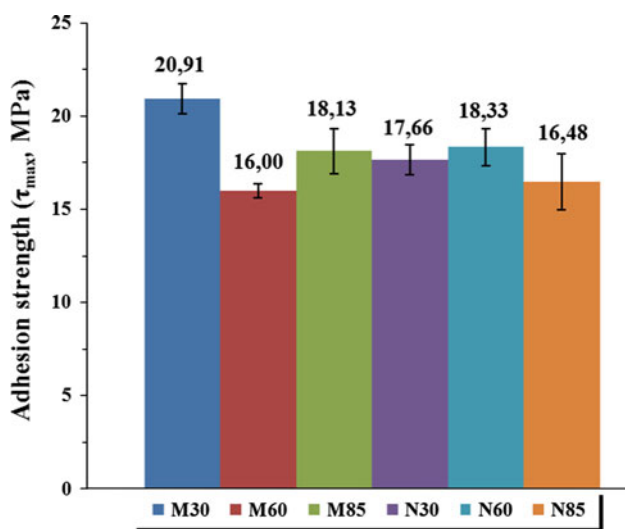

Fig. 4 Adhesion strengths of the HAP coatings

HA layers formed on the Al substrates. The highest adhesion strength was obtained as 20.91 MPa for M30 specimen. The obtained adhesion strengths presented in Fig. 4 are good enough to provide adequate implantations during orthopaedic operations. However, the high value of adhesion does not correspond to the best coating since such results should be evaluated together with the corrosion test results. It is seen from the adhesion test results that no correlation can be identified between the dipping time and particle size of HA. Therefore, the adhesion performances of the studied coatings are certainly related to the coat

thickness and microstructural properties such as porosity, cracks, crystal defects, internal stress, grain size etc. [3, 21, 25]. It is well known that Al is such material with a metallic bond and HA is a ceramic with a covalent bond. Thus, it is not possible to form a stable interface between the two materials without inter-compound bridging up. The internal stress was generated along the interface between substrate and coatings that also exaggerated the peeling with increasing the coating thickness [37, 38]. Although it was not analysed in this study, increasing the HA particle size also cause an increase in surface roughness of the coatings. In other words, bigger particle sizes can easily be damaged or fractured under fretting and sliding wear conditions.

3.3 Corrosion tests

Open circuit potential (OCP) of the specimens by using Ringer's solution were measured against time and the results are plotted in Fig. 5. As seen from the curves, E_{ocp} values increase as a function of time in all samples. This fact indicates that all specimens undergo spontaneous passivation due to spontaneously formed oxide film passivation of the coating surface. The increase in OCP values showed that within the first 15 min period, the rate of passive film formation had the highest value and later, the rate increase becomes less pronounced. The results showed that specimens coated with nano-scale HA had the noblest OCP values than micro-scale coatings.
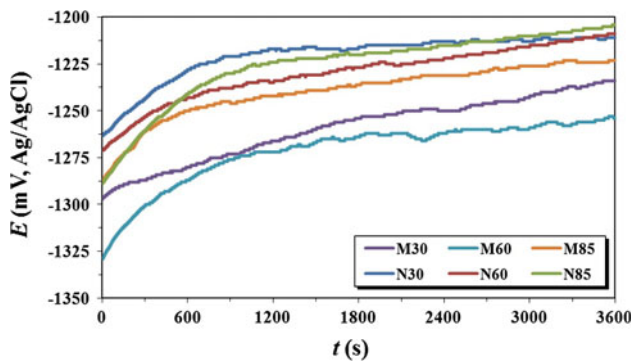
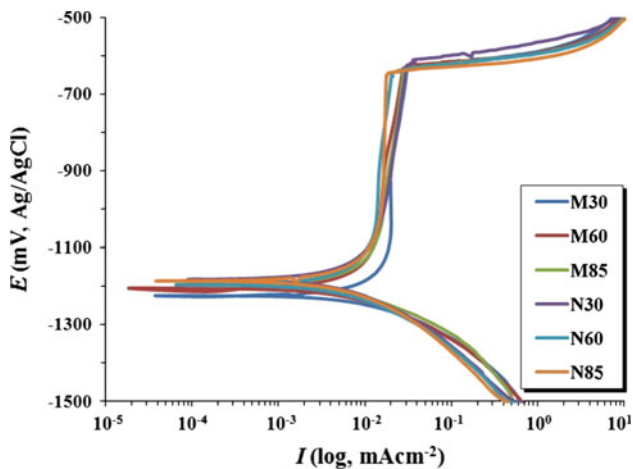**Fig. 5** Open circuit potential curves of the specimens in Ringer's solution

Fig. 6 Potentiodynamic polarization curves of the specimens in Ringer's solution

Table 2 Calculated corrosion parameters from PDS curves

Identification	E_{ocp} (mV)	E_{corr} (mV)	E_{pit} (mV)	E_{pp} (mV)	I_{corr} (μA/cm^2)
M30	−1233	−1227	−619	−1182	8.90
M60	−1253	−1213	−623	−1151	7.39
M85	−1223	−1201	−629	−1104	7.24
N30	−1211	−1182	−611	−1134	5.12
N60	−1209	−1199	−629	−1139	7.26
N85	−1204	−1186	−640	−1116	8.25

E_{ocp} open circuit, E_{corr} corrosion, E_{pit} pitting, E_{pp} passivity potentials, I_{corr} corrosion current density values

Potentiodynamic scanning (PDS) plots for the samples in Ringer's solution are shown in Fig. 6 and calculated corrosion parameters from these curves are given in Table 2. As can be seen from this figure, the PDS profiles are quite similar each other. All the studied samples reach their respective stable passive current densities as the potential increases and it indicates that a passive film formation is the present on the surfaces of all HABC coatings.
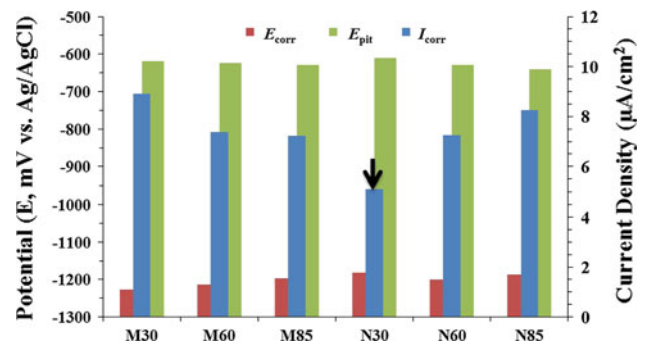

Fig. 7 Comparison of corrosion parameters derived from Table 2

The passive current densities remain almost unchanged inside their wide passive regions, indicating that their corrosion rates are in steady state and the passive films formed on the surfaces are stable. The presence of HABC coatings over the passive layer plays a dual role in preventing the release of metal ions and enabling the metal surface more bioactive. In this case, passivity (E_{pp}) and pitting (E_{pit}) potential and corrosion current density (I_{corr}) values can be used to characterize corrosion behaviour, and evaluate how effectively a passive film protects the coating from corrosion.

Figure 7 depicts the variation of the critical potentials and current density values versus coating thickness of the specimens. The small difference in corrosion potential values of the coatings are possibly related to the different HA particle size among these coatings. All specimens coated with nano-scale HA (N30, N60, N85) show more noble corrosion potential values as compared to its counterpart specimens coated with micro-scale HA (M30, M60, M85), suggesting that nano-HA coatings are higher corrosion resistant than micro-HA coatings. It can also be seen that the pitting potential values of coatings are close to each other and fluctuate between −611 and −640 mV. It is related to the consecutive formation and repassivation of microsize pits and is commonly called metastable pits in the micro-scale coatings [39]. However, it was observed that the current density values of the coatings had changed in a large gap. The lowest current density and the noble pitting potential values occurred in the thinnest coatings by nano scale HA (N30) (Fig. 7). In other words, it can be concluded that the N30 is the most resistant material to corrosion in Ringer's solution. Since it was observed that the coated specimens with nano scale HA produce less cracked structure than the coated specimens with micro scale HA (Figs. 2, 3). It is thought that this arises due to the cracks which are considered as weak regions in the coating structure [40].

As shown in Fig. 8 some surface cracks are visible for the coating of micro-scale HABC coatings after the corrosion tests took place at the same scale. Surface cracks for
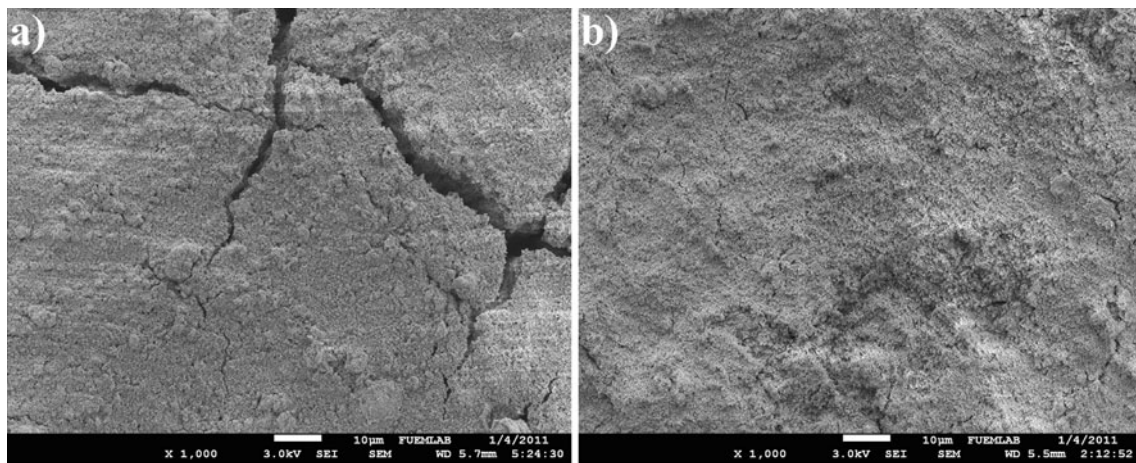
Fig. 8 SEM micrographs of the coating cracks after the corrosion tests: **a** M30, **b** N30
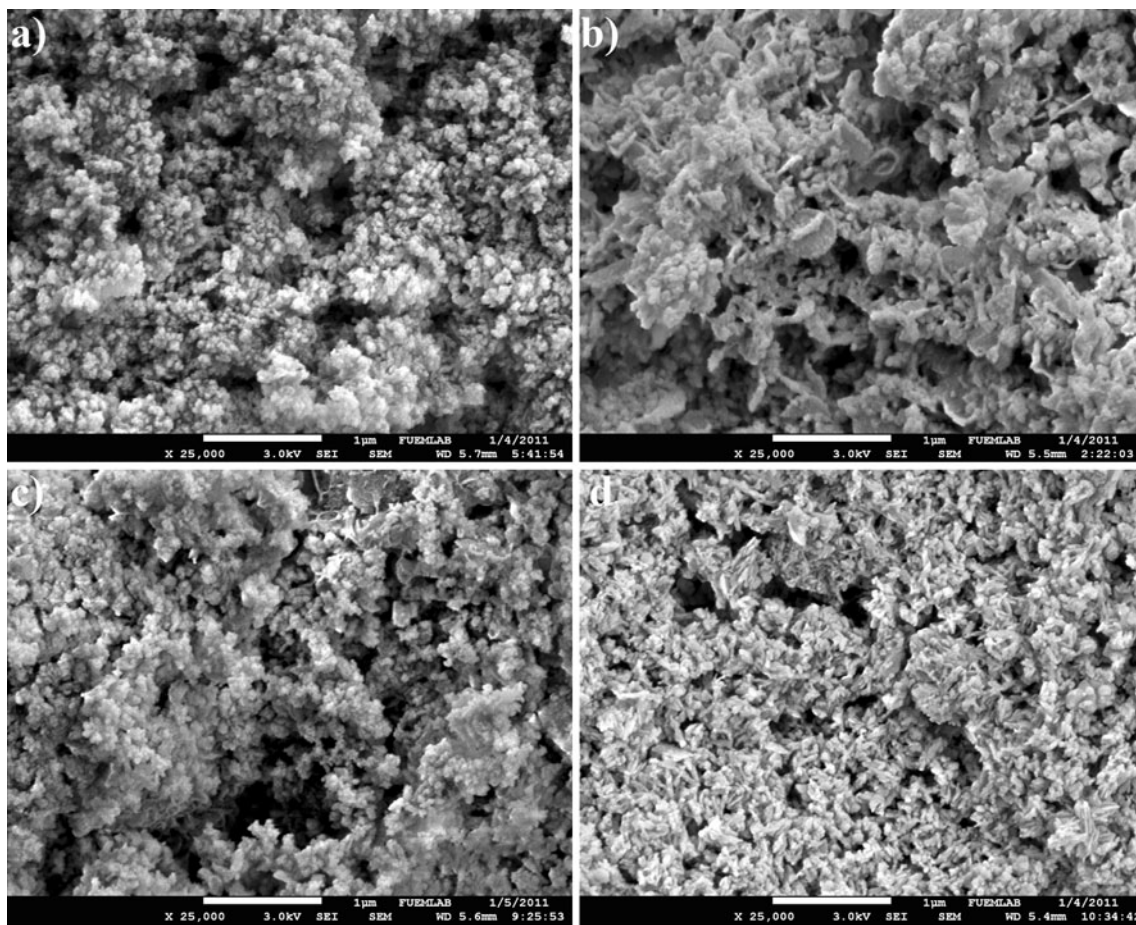

Fig. 9 Surface morphology of the HAP coatings after the corrosion tests: **a** M30, **b** N30, **c** M85, **d** N85

such coatings have a detrimental effect since the integrity of surface cannot be sustained for long periods. The cracks are generated in the coatings are the areas where the Ringer's solution is stagnating. Thus, these areas will act as anode and the environment of the cracks (crack free region of the HABC) will act as cathode. The interior crack pH will be decreased compared to the body pH and Cl^- ion concentration [41]. Consequently, interior crack potential will be anodized as a result of a decrease to negative values compared to the coating (or implant potential). This may
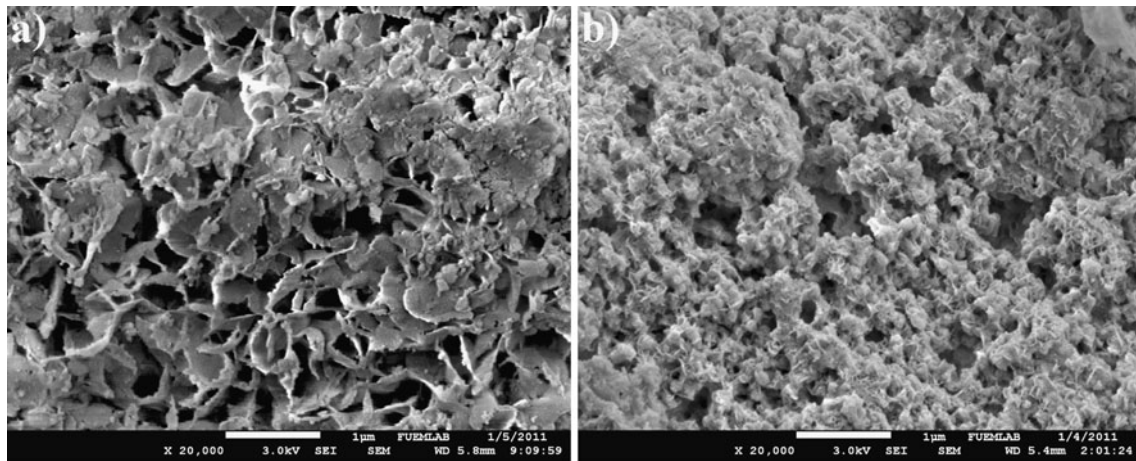
Fig. 10 SEM micrographs of the thickest coatings after the corrosion test: **a** M85 and **b** N85

cause an increase in the solubility of the coating layer. As a result, the corrosion mechanism will occur which is the most detrimental where the corrosion extended in depth. Some porosity is always required for biocompatible implants because living cells need the scaffold to proliferate and nutrition can be supplied as cells migrate into to the porous space [42]. As indicated in Fig 8b, the morphology of the specimen coated with nano scale HA (Fig. 8a) has a porous and crack free structure which is essential for implant longevity.

Figures 9 and 10 show the morphology and corrosion products that formed on the coating surfaces at low and high magnifications, respectively. It can be seen that, corroded surface exhibits a porous structure. The surface morphology of the coating, called as M30, was rough CaP crystals, which seem to be connected with each other forming a continuous sponge-like network (or the petal rose-like morphology). Black zones in Fig. 10a show the regions where dissolution process took place in depth after the corrosion tests. However, as can be seen in Fig. 10b, the pores constituted a continuous network for N30.

4 Conclusions

AA 6061-T4 alloy was coated by HA based bioceramic, HABC. The highest adhesion strength of the M30—HABC coating was obtained as 20.91 MPa. Such coatings exhibited a passive behaviour in Ringer's solution and nano-scale HA coatings (N30, N60, N85) showed more noble corrosion potential values as compared to micro scale HA at the same coat thicknesses, suggesting that nano-scale HA coatings have higher corrosion resistance than the micro-HA coatings. The N30 coatings produced the highest adhesion and corrosion resistance. It can also be concluded from the current results that the pitting potential values of

coatings are close to each other and fluctuate between the values of −611 and −640 mV.

References

1. Niinomi M (1998) Mater Sci Eng, A 243:231–236
2. Agraval CM (1998) Reconstr Metals Mater Soc 50:31–35
3. Aksakal B, Gavgali M, Dikici B (2010) J Mater Eng Perform 19:894–899
4. Perl DP (1985) Environ Health Perspect 63:149–153
5. Lee IU, Kim H, Kim S (2000) Surf Coat Technol 131:181–186
6. Singh R, Dahotre BN (2007) J Mater Sci Mater Med 18:725–751
7. Zhou YL, Niinomi M (2009) Surf Coat Technol 204:180–186
8. Kim H, Kim H, Knowles JC, Knowles J (2005) Am Ceram Soc 88:154–159
9. Buyuksagis A (2010) EJMT 7:1–11
10. Azem FA, Çakır A (2009) Anadolu Uni J Sci Technol 10:291–298
11. Balamurugan A, Balossier G, Kannan S (2007) Mater Sci Eng, C 27:162–171
12. Joon BP, Young KK (2000) Met Biomater 38:1–15
13. Ige OO, Umoru LE, Adeoye MO (2009) Trends Biomater Artif Organs 23:93–104
14. Williams DF (1994) J Bone Joint Surg 76:348–349
15. Karlsson M (2004) Nano-porous alumina, a potential bone implant coatings. Acta Universitatis Upsaliensis, Dissertation thesis, Uppsala
16. Shackelford JF, Alexander W (2001) Materials science and engineering handbook. CRC Press LLC, Boca Raton
17. Park JB, Lakes RS (2007) Biomaterials: an introduction, 3rd edn. Springer, USA
18. Wen CE, Xub W, Hub WY, Hodgsona PD (2007) Acta Biomater 3:403–410
19. Ak Azem F, Çakır A (2009) J Sol-Gel. Sci Technol 51:190–197
20. Stanishevsky AV, Holliday S (2007) Surf Coat Technol 202:1236–1241
21. Wang D, Bierwagen GP (2009) Prog Org Coat 64:327–338
22. Cameron SC, Karlis AG, Ben-Nissan B (1998) Biomaterials 19:2291–2296
23. Liu DM, Yang Q, Troczynski T (2002) Biomaterials 23:691–698
24. Cannillo V, Colmenares-Angulo J, Lusvarghi L, Pierli F (2009) J Eur Ceram Soc 29:1665–1667

25. Aksakal B, Hanyalıoğlu C (2008) J Mater Sci Mater Med 19:2097–2104
26. Kwok CT, Wong PK, Cheng FT, Man HC (2009) App Sur Sci 255:6736–6744
27. Mondragón-Cortez P, Vargas-Gutiérrez G (2004) Mater Lett 58:1336–1339
28. Zheng YF, Liu D, Liu XL, Li L (2008) Appl Surf Sci 255:512–514
29. Wu G, Zeng X, Li G, Yao S, Wang X (2006) Mater Lett 60:674–678
30. Davis JR (2000) Corrosion understanding the basics. ASM Int, Materials Park, Ohio
31. Shi J, Ding C, Wu Y (2001) Surf Coat Technol 137:97–103
32. Dorozhkin SV (2010) Acta Biomater 6:715–734
33. Karanjai M, Sundaresan R, Mohan TRR, Kashyap BP (2008) Mater Sci Eng, C 28:1401–1407

34. Putlyaev VI, Safronova TV (2006) Biomaterials 63:99–102
35. Regi MV, Calbet JMG (2004) Prog Solid State Chem 32:1–31
36. Mirhadi B, Mehdikhani B, Askari N (2011) Process Appl Ceram 5:193–198
37. Lin FH, Hsu YS, Lin SH, Sun JS (2002) Biomaterials 23:4029–4038
38. Thamaraiselvi TV, Rajeswari S (2005) Trends Biomater Artif Org 18:242–246
39. Alves APR, Santana FA (2004) Mater Sci Eng, C 24:693–696
40. AkAzem F, Çakır A (2008) Sci Technol 26:136–143
41. Topcuoglu M, Aydinol MK (2006) Xth Int corr symp 1-4:96–107
42. Cheng K, Gaorong H, Wenjian W, Haibo Q (2003) Mater Res Bull 38:89–97